Supplemental Materials
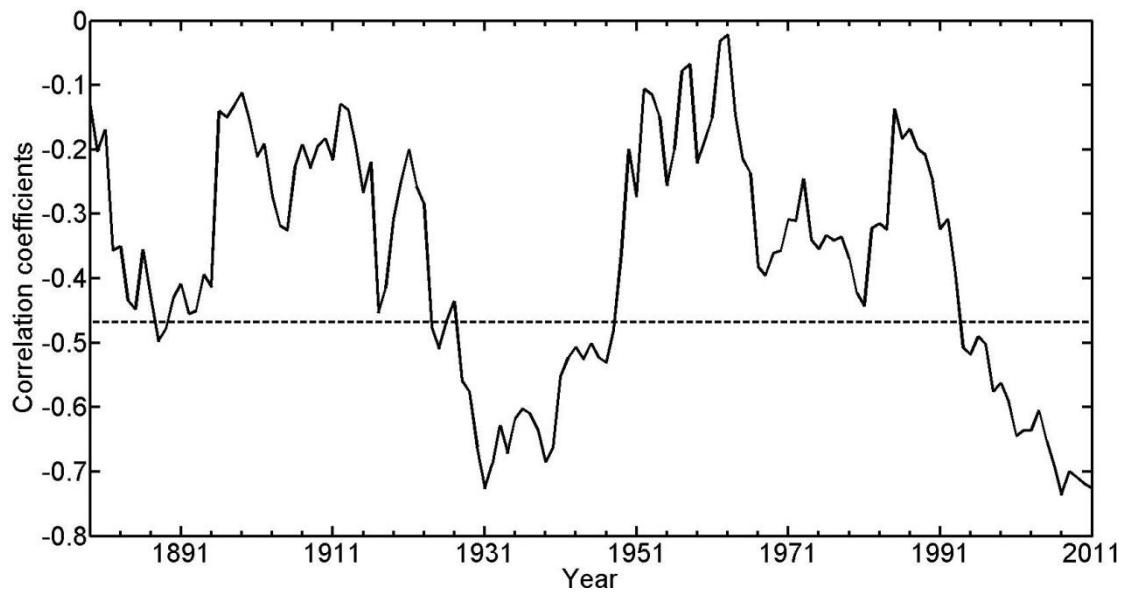
Figure S1. The 18-year moving correlations between the Niño3.4 and SASD indices from 1871 to 2020. The dashed line denotes the correlation coefficients with the above 95% confidence.
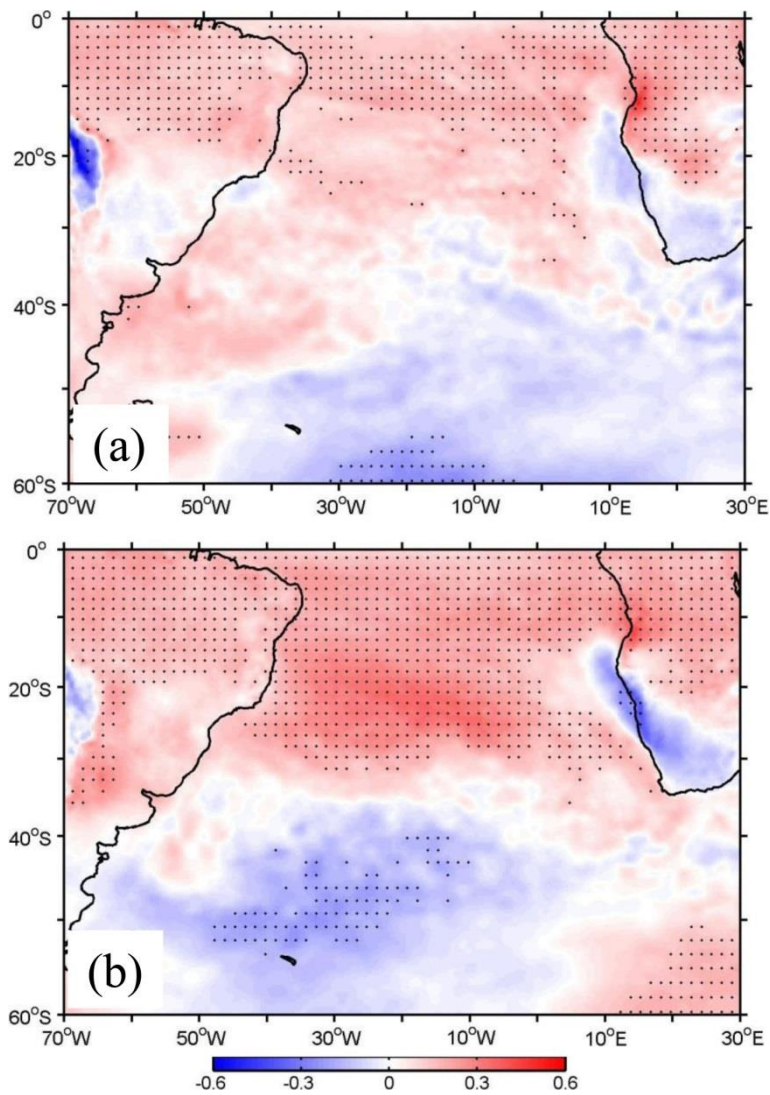
Figure S2. Regression maps of accumulated downward longwave radiation anomalies (10^6 W m^{-2}) onto the Niño 3.4 index for austral summer over the periods of 1979-1999 (a) and 2000-2020 period (b). Dotted regions denote the above 95% confidence level.
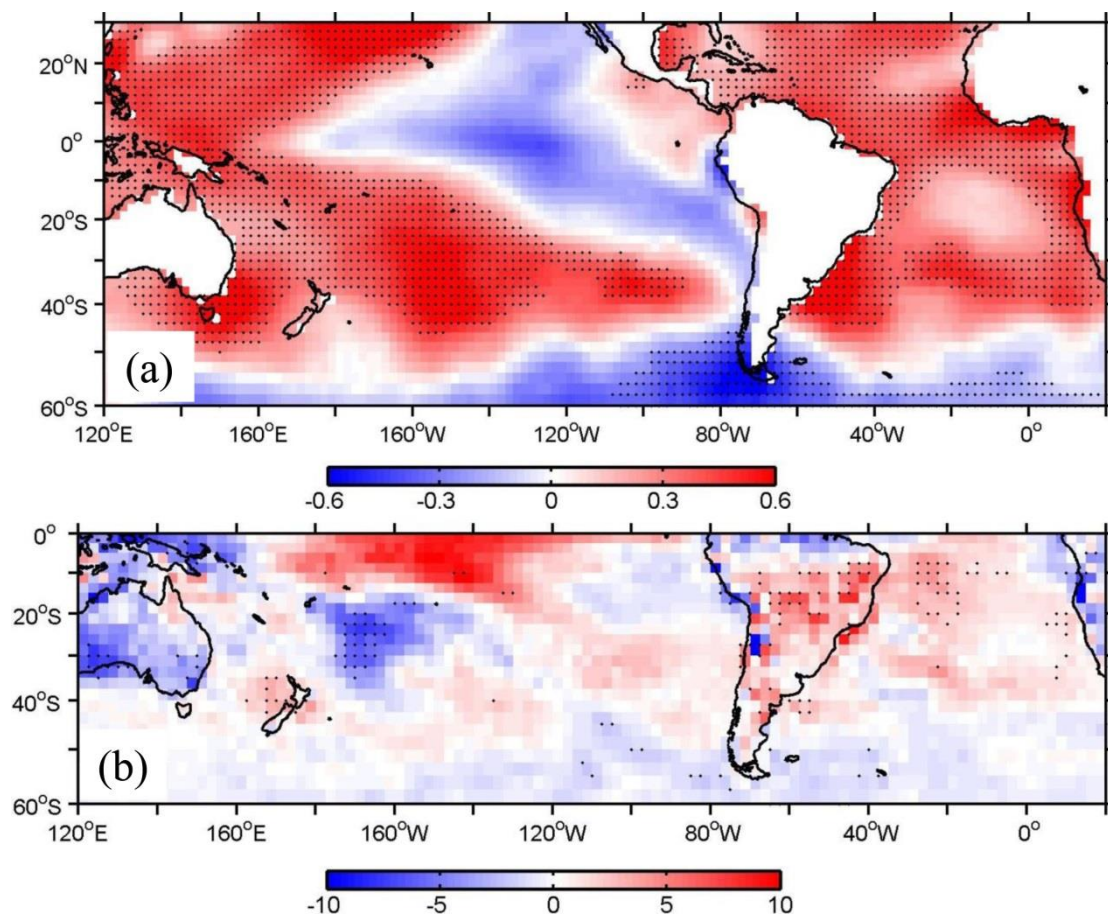
Figure S3. Difference of SST (^{o}C) (a) and OLR (W m^{-2}) (b) between the periods of 2000-2020 and 1979-1999. Dotted regions indicate the above 95% confidence level.
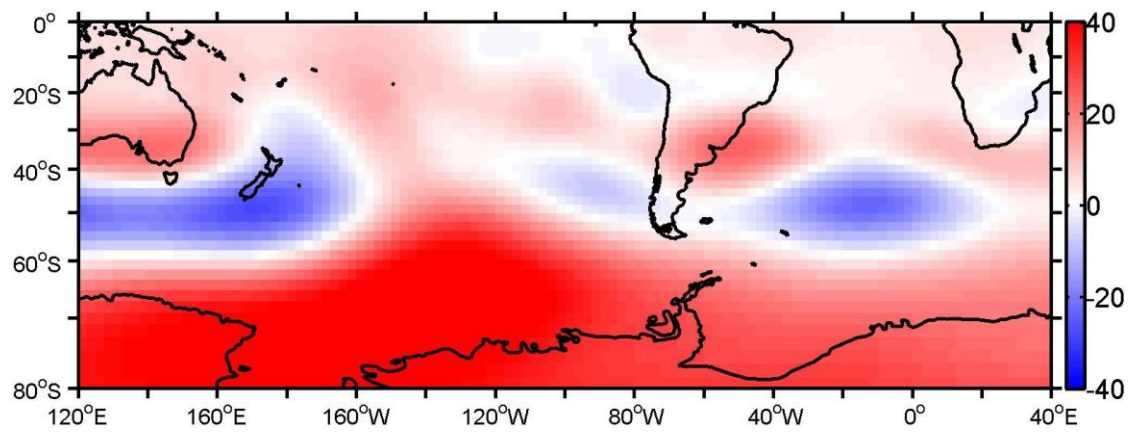
Figure S4. Anomalous 200-hPa geopotential height (gpm) of the idealized numerical experiment with a +2 ℃ SST anomaly introduced in the Indo-Pacific Warm Pool region (20 ℃S-40 ℃S, 180 °-140 ℃W) minus the control experiment using the CAM5 model.
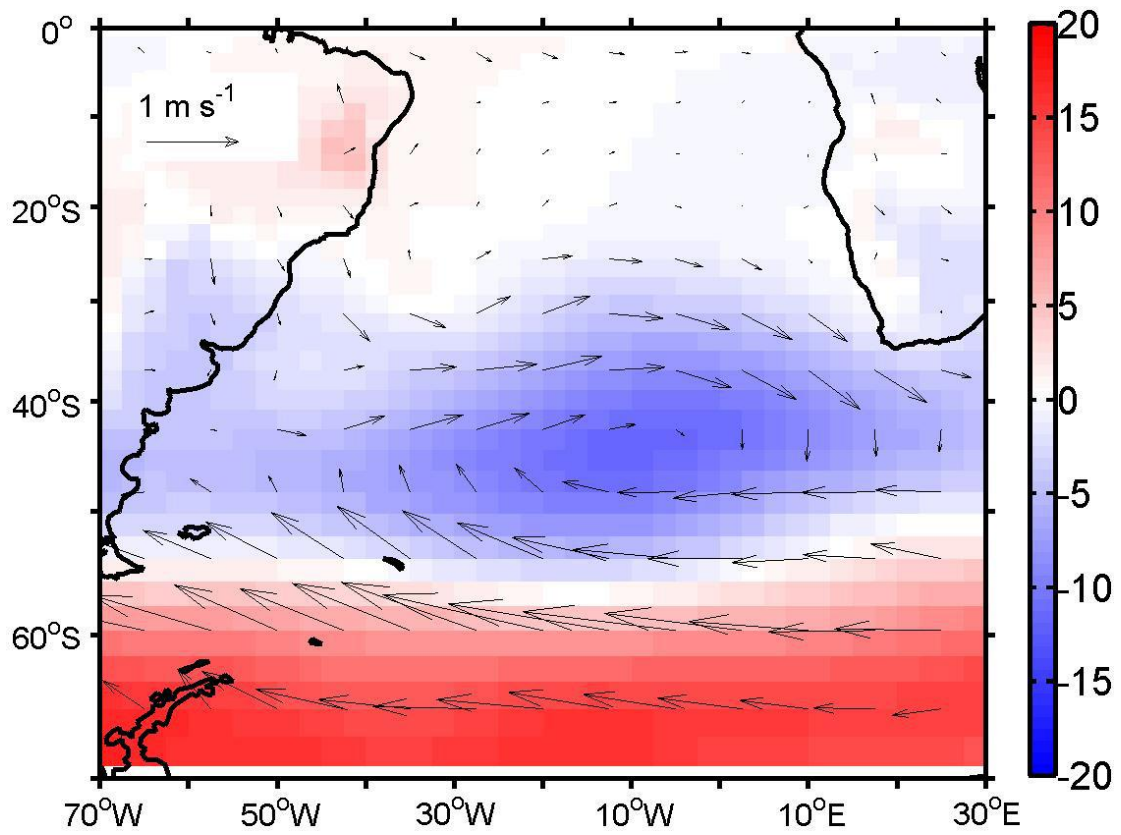
Figure S5. Anomalous 1000-hPa geopotential height (gpm) and wind field of the idealized idealized numerical experiment with a +2 ℃ SST anomaly introduced in the Indo-Pacific Warm Pool region (20 ℉S-40 ℉S, 180 °-140 ℉W) minus the control experiment using the CAM5 model.
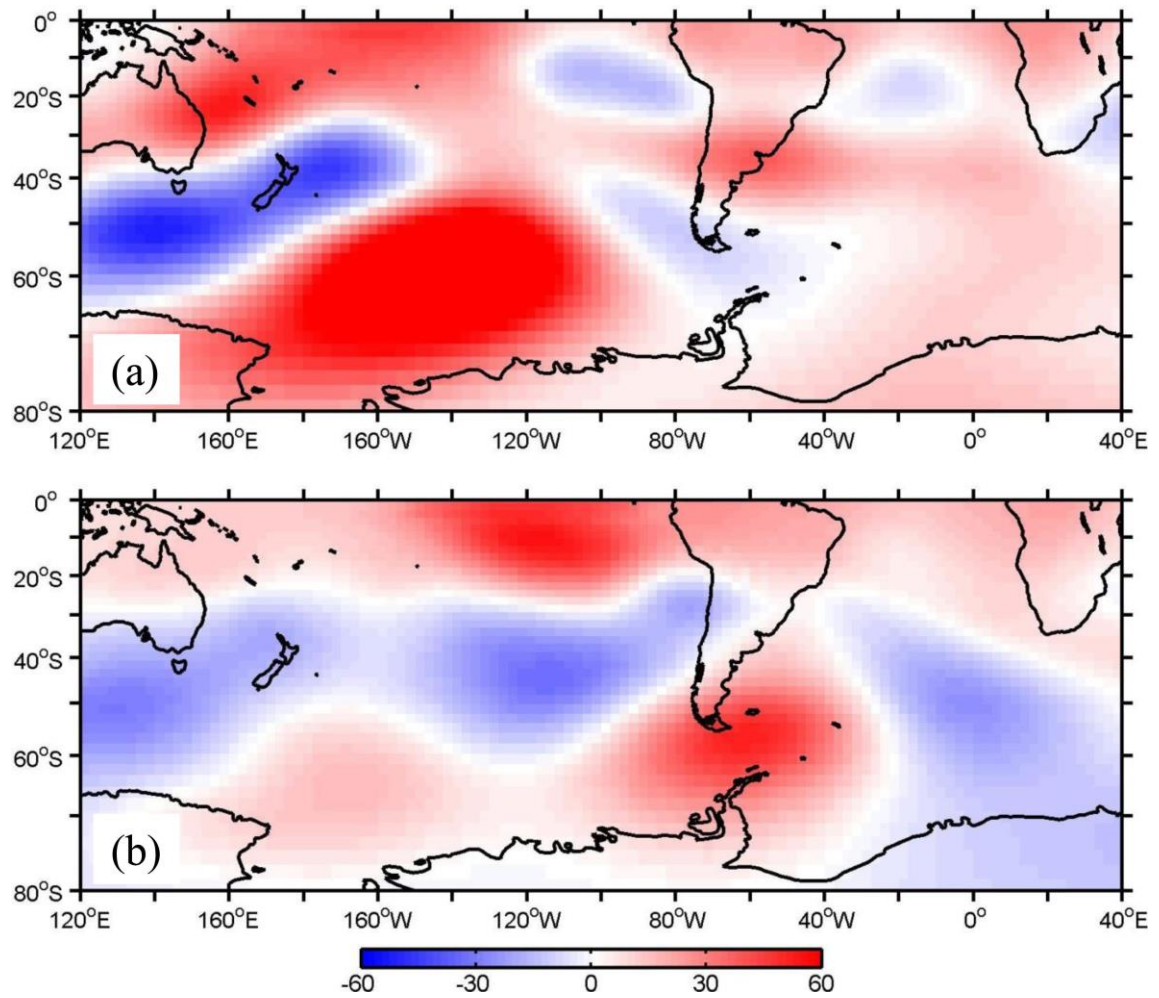
Figure S6. Anomalous 200-hPa geopotential height (gpm) of the idealized numerical experiment with +2°C SST over the Central Tropical Pacific (5°N-5°S, 160°E-150°W) (a) and +2°C SST over the East Tropical Pacific (5°N-5°S, 150°W-90°W) (b) minus the control experiment using the CAM5 model.
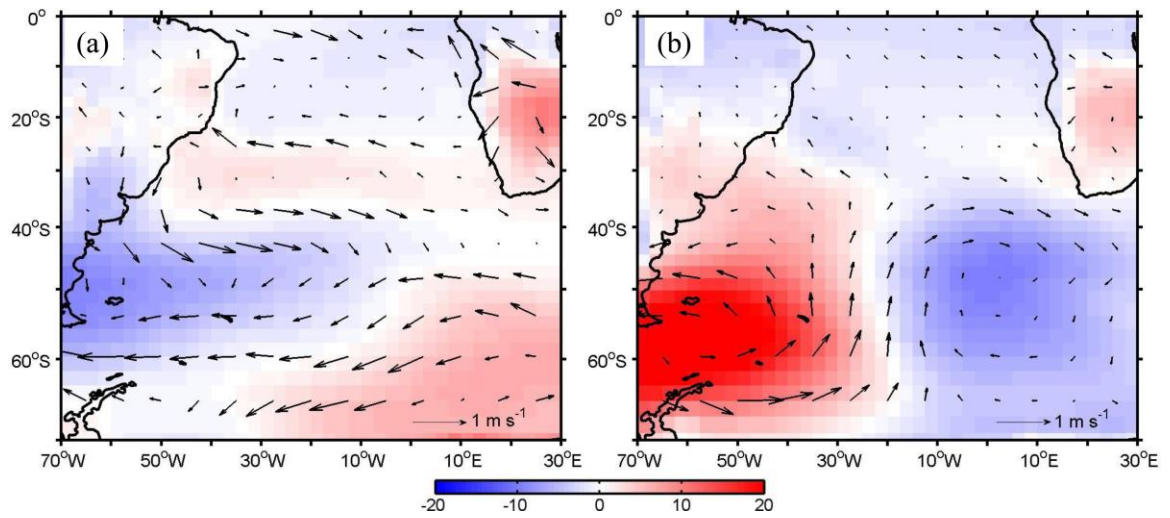
Figure S7. Anomalous 1000-hPa geopotential height (gpm) of the idealized numerical experiment with +2°C SST over the Central Tropical Pacific (5°N-5°S, 160°E-150°W) (a) and +2°C SST over the East Tropical Pacific (5°N-5°S, 150°W-90°W) (b) minus the control experiment using the CAM5 model.